Polyhedron 29 (2010) 1137–1143

Contents lists available at ScienceDirect

Polyhedron

journal homepage: www.elsevier.com/locate/poly

[Cp*Ru(*s*-indacene)RuCp*] and [Cp*Ru(*s*-indacene)RuCp*]$^+$: Experimental and theoretical findings concerning the electronic structure of neutral and mixed valence organometallic systems

D. Mac-Leod Carey [b], C. Morales-Verdejo [a], A. Muñoz-Castro [b], F. Burgos [c], D. Abril [d], C. Adams [a], E. Molins [e], O. Cador [f], I. Chávez [a], J.M. Manríquez [a,*], R. Arratia-Pérez [b], J.Y. Saillard [f]

[a] Facultad de Química, Pontificia Universidad Católica de Chile, Avda. Vicuña Mackenna 4860, Santiago, Chile
[b] Departamento de Ciencias Químicas, Universidad Andrés Bello, República 275, Santiago, Chile
[c] Facultad de Ciencias Forestales, Universidad Austral de Chile, Avda. Los Laureles s/n, Valdivia, Chile
[d] Instituto de Ciencias Básicas, Universidad Católica del Maule, Avda. San Miguel 3605, Talca, Chile
[e] Institut de Ciencia de Materials de Barcelona (CSIC), Campus UAB, 08193 Bellaterra, Spain
[f] Laboratoire de Chimie du Solide et Inorganique Moléculaire UMR CNRS 6511, Institut de Chimie de Rennes, Université de Rennes 1, 35042 Rennes Cedex, France

ARTICLE INFO

Article history:
Received 24 June 2009
Accepted 2 December 2009
Available online 5 December 2009

Keywords:
s-Indacene
Ruthenium
Organometallic
Electron transfer
Mixed valence
DFT

ABSTRACT

The reaction of 2,6-diethyl-4,8-dimethyl-*s*-indacenyl-dilithium (Li_2Ic') with $[Cp^*RuCl]_4$ gives the organometallic binuclear bis-pentamethylcyclopentadienyl-ruthenium-*s*-indacene complex, $[\{Cp^*Ru\}_2Ic']$ (**1**, Ic′ = 2,4-diethyl-4,8-dimethyl-*s*-indacene), in high yields. The subsequent oxidation of **1** with a ferricinium salt ($[Fc]^+[BF_4]^-$) gives the mixed valence compound $[\{Cp^*Ru\}_2Ic']^+[BF_4]^-$ (**1**$^+$). Compound **1** was structurally characterized by X-ray crystallography, finding that both {Cp*Ru} fragments are coordinated to opposite sites of the Ic′ ligand. The structural and electronic features of **1** and **1**$^+$ have been rationalized by Density Functional Theory (DFT) calculations, which suggest that both metallic centers get closer to the Ic′ and subtle electronic reorganizations occurs when chemical oxidation takes place. Cyclic voltammetry and ESR experiments suggest a high electronic interaction between the metallic centers mediated by the Ic′ bridging ligand. Time dependent DFT (TD-DFT) calculations were carried out to understand and assign the intervalence band present in the mixed-valent specie (**1**$^+$). The main achievement of this article is to feature the relationship of the experimental data with the computational results obtained with the Amsterdam Density Functional package (ADF). Both experimental and theoretical facts demonstrate that the mixed valence system (**1**$^+$) is a delocalized one, and it can be classified as a Class III system according to the Robin & Day classification.

1. Introduction

Organometallic polynuclear compounds bridged by spacer ligands provide an interesting research area, due to the possibility of dealing with metallic centers which may communicate depending on the nature of the ligand, and of the chosen metallic fragments [1,2]. In the particular case of *s*- and *as*-indacene spacer molecules, several articles have been published describing the synthetic procedure using metallic fragments such as Cp^*M^{II}– (M = Fe, Co, Ni) (Cp^* = pentamethylcyclopentadienyl) [3], $(CO)_3M^I$ (M = Fe,Co) [4,5], $(COD)Rh^I$– (COD = 1,5-cyclooctadiene) [6], amongst others [7,8] to produce homobimetallic systems. Also a recent stepwise procedure to synthesize heterobimetallic systems containing Cp^*M^{II}– (M = Fe, Ru, Co, Ni) and $(COD)Rh^I$-metallic fragments [9] has been reported.

To date, the only known theoretical calculations describing the electronic structure of *anti*-$[\{CpM\}_2(Ic)]$ diamagnetic complexes (Cp = cyclopentadienyl; M = Fe, Co, Ni; Ic = *s*-indacene) were done at the extended Hückel level [10].

It has been experimentally demonstrated that these type of systems present a high degree of interaction between the metallic centers, but a detailed study which may explain the electronic mechanism that allows this interaction, has not been reported for *anti*-$[\{CpM\}_2(Ic)]$ systems, i.e. both CpM fragments at opposite sides of the Ic ligand.

The first concern of this article is to report the synthesis of a ruthenium binuclear organometallic system *anti*-$[\{Cp^*Ru\}_2Ic']$ (**1**, Ic′ = 2,4-diethyl-4,8-dimethyl-*s*-indacene) and its corresponding mixed-valent derivative *anti*-$[\{Cp^*Ru\}_2Ic']^+[BF_4]^-$ (**1**$^+$), together with the structural characterization by means of single-crystal

* Corresponding author. Tel.: +56 2 6864393.
E-mail address: jmanriqm@uc.cl (J.M. Manríquez).

0277-5387/$ - see front matter © 2009 Elsevier Ltd. All rights reserved.
doi:10.1016/j.poly.2009.12.002

X-ray diffraction, electrochemical analysis, spectroscopical studies and theoretical calculations at DFT level of theory. The degree of communication that exists between the two metallic centers through the Ic′ bridging ligand was studied, engaging all the experimental information with the theoretical analysis in order to rationalize and understand which are the main features that enable the electronic delocalization in the mixed valence system.

2. Experimental

2.1. General experimental details

All manipulations were carried out under an atmosphere of nitrogen using standard Schlenck techniques or in a Vacuum Atmosphere glove box under nitrogen. Solvents used were predried and distilled with standard techniques using appropriate drying agents [11]. The following compounds were prepared according literature methods: 1,5-dihydro-2,6-diethyl-4,8-dimethyl-*s*-indacene ($Ic'H_2$) [12], $[Cp^*RuCl]_4$ [13]. NMR samples were made up in the dry box, and the sample tubes were sealed with septa. ^1H and $^{13}C\{1H\}$ NMR spectra were recorded with a Bruker Avance 400 MHz instrument by using C_6D_6 as solvent at 25 °C, the spectra were referenced internally, using the residual protio solvent resonances, to tetramethylsilane ($\delta = 0$ ppm). Mass spectra were measured with a Hewlett–Packard HP 5989A in the electron impact mode (70 eV). Elemental analyses (C and H) were made with a Fisons EA 1108 microanalyzer. Cyclic voltammetry experiments were performed in an airtight three-electrode cell connected to an argon line. The reference electrode was an SCE (saturated calomel electrode, SCE versus Fc/Fc^+ couple is 430 mV). The counter electrode was a platinum wire, and the working electrode was a platinum disc with diameter of ca. 3 mm. The currents and potentials were recorded with a Pentium II 350 MHz processor, with a BAS CV-50 Voltammetric Analyzer Potentiometer. Each electrochemical experiment employed the first fraction of distilled CH_2Cl_2, which was collected over phosphorus pentoxide and heated at reflux once again. The supporting electrolyte, tetrabutylammonium tetrafluoroborate (TBATFB, $[NBu_4]^+[BF_4,]^-$), was dried under vacuum for 3 h prior use. ESR spectra were recorded on a Brucker ER 200 instrument with frequency meter EIP.

2.2. Synthesis of the binuclear systems

2.2.1. anti-[Cp*Ru–Ic′–RuCp*], 1

A solution of $Ic'H_2$ (0.50 g, 2.10 mmol) in tetrahydrofuran (THF, 15 mL) was cooled to −80 °C. A hexane solution of *n*-butyllithium (*n*-BuLi, 1.6 mol L^{-1}, 2.63 mL, 4.20 mmol) was then added drop wisely over the $Ic'H_2$ solution. The reaction mixture was allowed to warm to room temperature and stirred by 30 min, producing the dilithiated salt of Ic′ ($Ic'Li_2$). The mixture was then cooled to −80 °C, and a solution of the ruthenium tetramer ($[Cp^*RuCl]_4$, 1.14 g, 1.05 mmol) in tetrahydrofuran (20 mL) was added *via* syringe. Then, the solution was allowed to warm to room temperature and stirred by 2 h, the solvent was removed until dryness. The solid residue was extracted with toluene, filtered to eliminate the solid lithium chloride formed, washed 3 times with toluene, and dried under vacuum. A mixture of the binuclear and mononuclear species is obtained. This mixture was washed with pentane in order to remove the mononuclear specie. The binuclear compound was obtained then as green crystals unstables to air. Yield 0.78 g, 53%.

Anal. Calc. for $C_{38}H_{50}Ru_2$ (708.53 g mol^{-1}): C, 64.36; H, 7.11. Found: C, 64.04; H. 6.75.

^1H NMR (C_6D_6, δ ppm, 293 K): 4.92 (s, 4H, $CH_{(1,3,5,7\text{-}Ic')}$); 1.56 (s, 30H, CH_3–$C_{(Cp^*)}$); 2.45 (s, 6H, CH_3–$C_{(4,8\text{-}Ic')}$); 2.29 (q, 4H, CH_3–CH_2–$C_{(2,6)}$, $^3J_{H-H}$ = 7.48 Hz); 1.08 (t, 6H, CH_3–CH_2–$C_{(2,6)}$, $^3J_{H-H}$ = 7.48 Hz). $^{13}C\{1H\}$ NMR (C_6D_6, δ ppm, 293 K): 11.16 (10C, CH_3–$C_{(Cp^*)}$); 81.46 (10C, CH_3–$C_{q(Cp^*)}$); 63.45 (4C, $CH_{(1,3,5,7\text{-}Ic')}$); 15.73 (2C, CH_3–$C_{(4,8\text{-}Ic')}$); 14.80 (2C, CH_3–CH_2–$C_{(2,6)}$); 22.82 (2C, CH_3–CH_2–$C_{(2,6)}$); 100.34 (2C, CH_3–CH_2–$C_{q(2,6)}$); 120.28 (2C, CH_3–$C_{q(4,8\text{-}Ic')}$); 99.01 (4C, $C_{q(9,10,11,12\text{-}Ic')}$). MS (FAB): *m/z* 710 ($M^{\cdot+}$, 100%), 695 ($M^{\cdot+}-CH_3$) (Scheme 1).

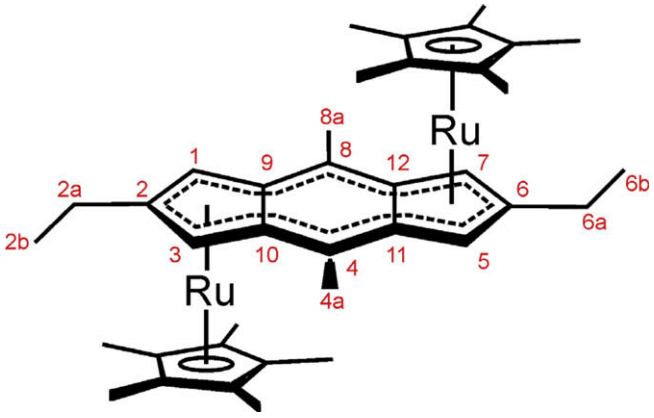

Scheme 1. Labelling scheme for Table 1 and NMR assignation.

2.2.2. anti-[Cp*Ru–Ic′–RuCp*]$^+$[BF_4]$^-$, 1^+

$[FeCp_2]^+[BF_4]^-$ (63 mg, 0.231 mmol) and **1** (180 mg, 0.254 mmol) were dissolved in tetrahydrofuran (15 mL) the mixture was stirred at room temperature by 4 h resulting in the formation of a brown precipitate, the mixture was filtered and the insoluble material was washed with diethyl ether to remove all the ferrocene and dried *in vacuo*. The solid was recrystallized by slow diffusion of diethyl ether into a concentrated CH_2Cl_2 solution of **2**. Brown crystals were observed within 24 h. The crystals were filtered, washed with diethyl ether and dried *in vacuo*. Yield 174 mg, 86%.

Anal. Calc. for $C_{38}H_{50}Ru_2BF_4$ (795.52 g mol^{-1}): C, 57.36; H, 6.33. Found: C, 57.30; H. 6.10. MS (FAB): *m/z* 798 ($M^{\cdot+}$, 100%), 695 ($M^{\cdot+}-CH_3$).

2.3. Crystal structure determination

Suitable crystals of **1** for X-ray diffraction were obtained from a toluene/pentane solution. A single crystal of approximate dimensions 0.43 × 0.21 × 0.19 was used for the cell determination and data collection. Lattice constants were determined by least-squares fitting of the setting angles of 25 reflections. Data were recorded using the ω–2θ scan mode up to θ of 26.98°. All intensities were corrected for Lorentz polarization and absorption effects (empirical ψ scan, maximum and minimum transmission were 0.8405 and 0.6862, respectively). The structure was solved by direct methods using SHELXS-86 [14] and refined by full-matrix least squares methods on F^2 over the complete set of data using SHELXL-97 [15]. Anisotropic thermal parameters were refined for the non-hydrogen atoms, and the hydrogen atoms were introduced in calculated positions. Crystal data, data collection and refinement details are given in Supplementary data. All X-ray diffraction data were collected at 294(2) K.

3. Computational details

Density Functional Theory (DFT) calculations were carried out by using the Amsterdam Density Functional (ADF) package [16]. Geometry optimizations were done *via* the analytical energy gradient method implemented by Verluis and Ziegler employing the

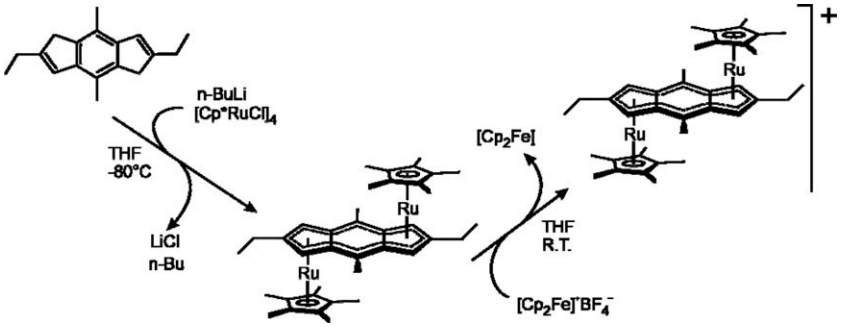

Scheme 2. Synthetic route to **1** and $\mathbf{1}^{+}$ complexes.

Local Density Approximation (LDA) within the Vosko, Wilk and Nusair parametrization (VWN) for the local exchange correlation [17], nonlocal corrections proposed by Perdew–Wang in 1991 [18] were incorporated into the exchange and correlation functionals, and were treated by a fully self-consistent method. Scalar relativistic effects were taking into account *via* the Zero Order Regular Approximation (ZORA) Hamiltonian [19,20]. For the calculations we used the standard ADF IV basis set [21], which is an uncontracted triple-ζ STO basis set for H 1s, C 2s, Ru 4d; augmented with one 3d single polarization function for C atoms, a 2p single polarization function for H atoms and a 5p single polarization function for Ru atoms. Spin-unrestricted calculations were performed for the open-shell systems. The molecular structure described here have been characterized as the energy minima through calculations of normal mode vibrational frequencies, which were performed at the optimized geometry *via* second derivatives of the total energy with respect to the internal coordinates as implemented in the ADF code [22,23]. Some imaginary frequencies were founded around $-60\ cm^{-1}$ ($60i\ cm^{-1}$) for **1** and **2** which can be attributed to the free rotation of the Cp* over the metal atom. The TD-DFT calculations have been performed on the optimized geometries with the ADF-RESPONSE module [24] which is an extension of the ADF package. We employ for these response calculations the exchange-correlation model potential SAOP [25,26], which is constructed with a statistical average of different model potential for the occupied orbitals. SAOP was specially designed for the calculation of optical properties.

4. Results and discussion

4.1. Synthesis and characterization

Our synthetic strategy for the preparation of the bimetallic complexes incorporating the Ic′ ligand was salt elimination, using the dianion of the bridging ligand. Several substituted *s*-indacene dianions has been employed successfully in the synthesis of several homobimetallic complexes as [(Cp*M)$_2$Ic] (M = Fe, Co, Ni) [3], [(RhCOD)$_2$Ic] (COD is 1,5-cyclooctadiene) [7], whereas other

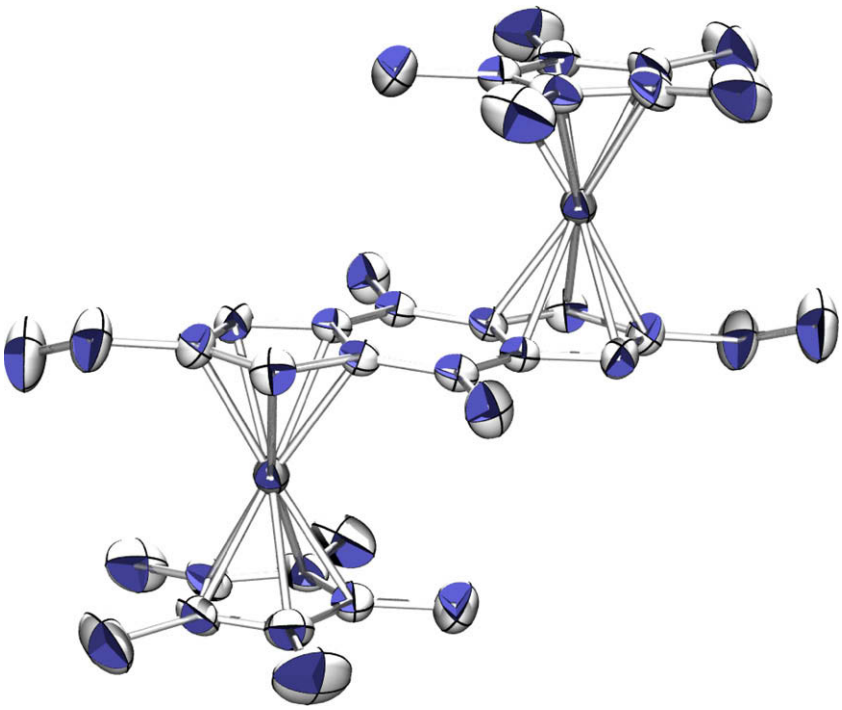

Fig. 1. Molecular representation in the crystal structure of [{Cp*Ru}$_2$Ic′] (**1**). Displacement ellipsoides drawn at 40% level. Hydrogen atoms not shown, for the sake of simplicity.

authors have employed the neutral 12 π *s*-indacenes derivatives in the synthesis of bimetallic complexes [{(CO)$_3$M}$_2$(Ic″)] {M = Fe, Co; Ic″ = tetra-1,3,5,7-*tert*-buthyl-*s*-indacene} [4,5]. For the preparation of the dianion, the dihydro-*s*-indacene was doubly deprotonated with two equivalents of *n*-butyllithium, as shown in Scheme 2. Once the dianion is prepared, it can be coupled to the metallic fragment *via* salt elimination. The bimetallic derivative **1** is chemically oxidized with ferricinium tetrafluoroborate, giving the mixed valence specie **1**$^+$. These two reactions provide a high yield (50–85%) and NMR spectroscopy showed only a single isomer to be present in **1**.

Suitable crystals of **1** for single-crystal X-ray diffraction analysis were grown by cooling a concentrated solution of toluene and pentane diffusion. The structure determination revealed that, in the solid state, the molecule is centrosymmetric and the Cp*Ru organometallic fragments are located in an *anti* coordination mode to opposite sides of the Ic′ ligand. This can be attributed to the steric hindrance provided by the two Cp* moieties.

The Ortep representation showed in Fig. 1, evidences that both metallic centers present a nearly perfect η [5] hapticity with Cp* and Ic′ ligands. The Ic′ centroid distances to the ruthenium atoms are 1.847 Å. Furthermore the distance between the Ru and Cp* centroids are 1.780 Å, which provide evidence that ruthenium has a stronger coordination to Cp* than the Ic′ ligand. These values are comparable with those found for *syn*-[Cp*RuIc′RhCOD] [9] which are 1.843 and 1.775 Å for the respective Ru–Ic′ and Ru–Cp* centroids, and can be compared with 1.840 and 1.794 Å for the respective Ru–Pentalenyl and Ru–Cp* centroids in the *anti*-[Cp*Ru(Pentalenyl)RhCOD] [27] complex. The distance data related to the coordination mode of the Ru atom in complex **1** it does not present significant differences compared with those from literature.

4.2. Redox behaviour of *1*

It can be seen in Fig. 2 that the cyclic voltammogram presents two quasireversible monoelectronic redox process, the first at $E_{1/2}$ = −388 mV corresponding to the [{Cp*Ru}$_2$Ic′]^0/[{Cp*Ru}$_2$Ic′]$^{1+}$ couple and the other at $E_{1/2}$ = +405 mV corresponding to [{Cp*Ru}$_2$Ic′]$^{1+}$/[{Cp*Ru}$_2$Ic′]$^{2+}$ couple, using as reference a saturated calomel electrode (SCE). The difference of potential between the two oxidation picks is $\Delta E_{1/2}$ = 793 mV, giving a high comproportionation constant

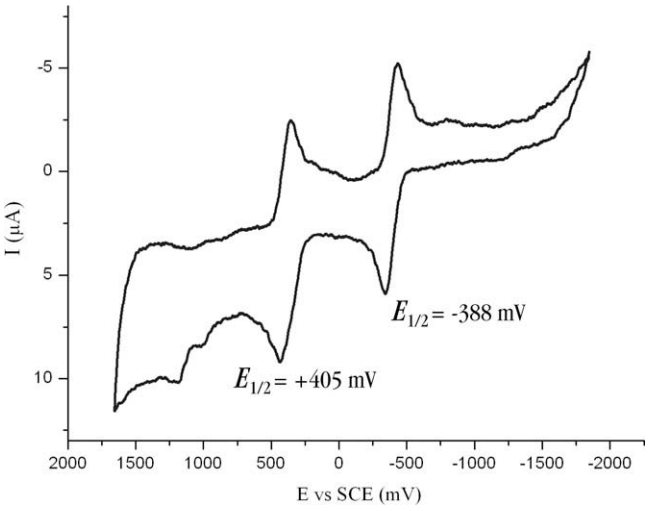

Fig. 2. Cyclic voltammogram of **1** 3.0 mM in CH_2Cl_2 (0.1 [*n*-Bu$_4$N]$^+$[BF$_4$]$^-$; scan rate 0.1 V s^{-1}).

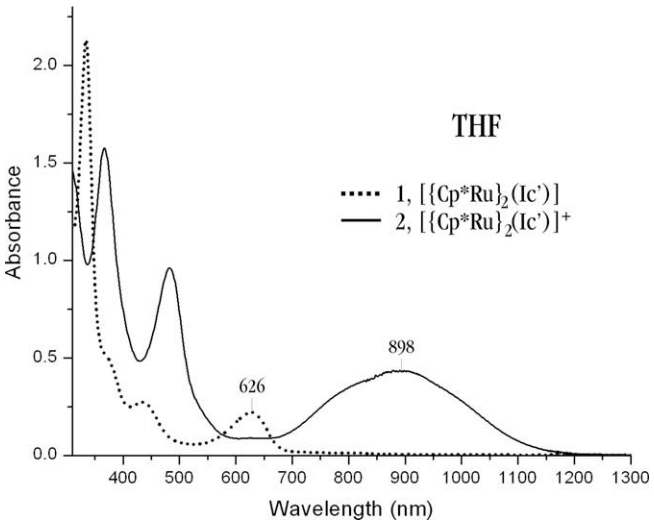

Fig. 3. UV–Vis-NIR spectra of **1** and **1**$^+$ in THF solution (∼1 × 10^{-5} M).

(Kc = 2.55 × 10^{13}) suggesting a high stability for the intervalence system **1**$^+$. This significative difference between those oxidation potentials give us the indication of a strong communication between the two metallic centers through the *s*-indacene bridge [28–31]. This can be compared with the [Cp*Ru-Pentalene-RuCp*] reported by Manríquez et al. [3] in which ΔE = 500 mV. Allowing us to suggest that the Ic′ ligand grants a stronger communication than pentalene.

4.3. Electronic spectra

The UV–Vis-NIR spectra of **1**$^+$ shows the presence of an intervalence band, between 680 and 1150 nm, with λ_{max} at 898 and 901 nm in THF and DCM solution respectively, which was not observed in the spectra of the neutral specie **1** (see Fig. 3). This band shows us the unambiguous existence of a strong communication between the two metallic Ru centers. If we compare this intervalence band with its analogous [Cp*Ru-Pentalene-RuCp*]$^+$[BF$_4$]$^-$ (1219 nm in CD_2Cl_2) or its isoelectronic analogous [Cp*Fe-*s*-indacene-FeCp*]$^+$[BF$_4$]$^-$ (1708 nm in CD_2Cl_2) [3], it can be deduced that,

Table 1
Bond lengths (Å) from the crystal structure of **1** compared with corresponding calculated distances[a] in the compounds **I** and **I**$^+$.

	1	**I**	**I**$^+$
Ru–C$_1$	2.191(4)	2.242	2.249
Ru–C$_2$	2.210(4)	2.254	2.276
Ru–C$_3$	2.185(4)	2.229	2.233
Ru–C$_9$	2.246(4)	2.376	2.299
Ru–C$_{10}$	2.241(3)	2.378	2.297
Ru–Centroid a in Ic′	1.847	1.940	1.910
Ru–Cp* ring average	2.162	2.216	2.233
Ru–Cp* ring range	2.147–2.172	2.197–2.229	2.214–2.254
Ru–centroid in Cp*a	1.780	1.845	1.866
C$_2$–C$_1$	1.430(6)	1.434	1.433
C$_2$–C$_3$	1.420(5)	1.434	1.432
C$_1$–C$_9$	1.434(5)	1.449	1.447
C$_3$–C$_{10}$	1.434(5)	1.450	1.445
C$_4$–C$_{10}$	1.420(5)	1.409	1.415
C–C Cp* average	1.425	1.442	1.443
C–C Cp* range	1.415–1.434	1.435–1.452	1.439–1.448

[a] Non-listed data are redundant distances. The atom labels are referred to Scheme 1, which could be found in Section 2.

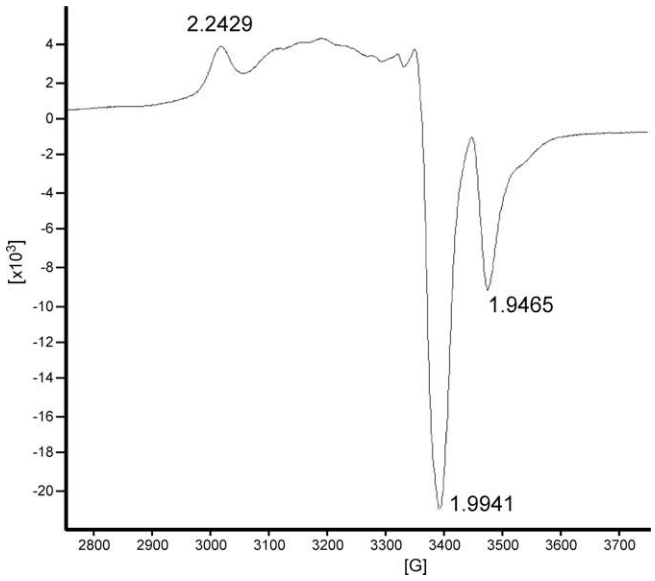

Fig. 4. EPR spectra of $\mathbf{1}^+$ at 4 K.

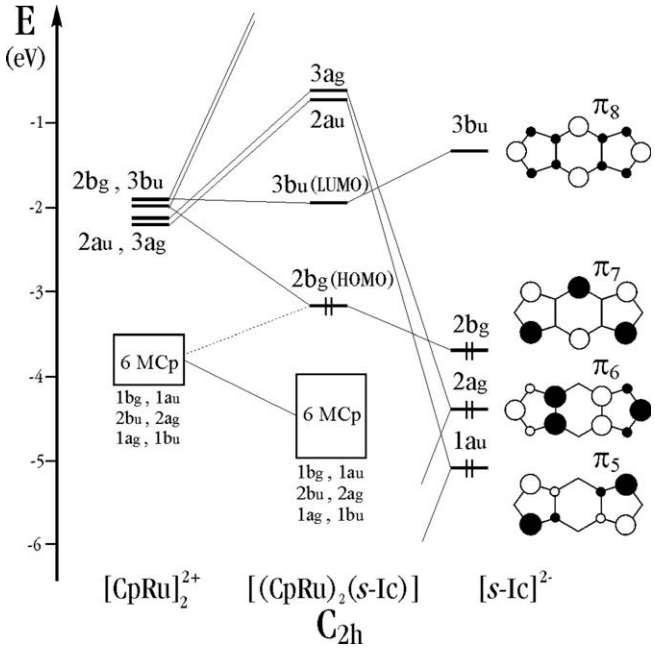

Fig. 5. MO interaction diagram of a simplified model of **1**, [{CpRu}$_2$(*s*-Ic)].

in the case of $\mathbf{1}^+$, the energy requirements to accomplish the electron transfer are bigger.

4.4. Electron paramagnetic resonance

Here, two possibilities for system $\mathbf{1}^+$ can be attained, to be in presence of a valence trapped system in which a combination of two distinct Ru centers, a diamagnetic EPR silent Ru^{II} and the paramagnetic counterparts Ru^{III} which exhibits a high degree of g-tensor anisotropy. In the other expected behaviour, $\mathbf{1}^+$ exhibit two equivalent Ru centers (valence detrapped), thus a low value of g-tensor anisotropy is expected for a delocalized system [3].

The 4 K EPR spectra of $\mathbf{1}^+$ presented in Fig. 4 shows a significantly reduced g-tensor anisotropy of $\Delta g = |g_{\|} - \hat{g}_{\perp}| = 0.28$ when compared with its isoelectronic analogous $[\{Cp^*Fe\}_2(s\text{-Indacene})]^+[BF_4]^+$

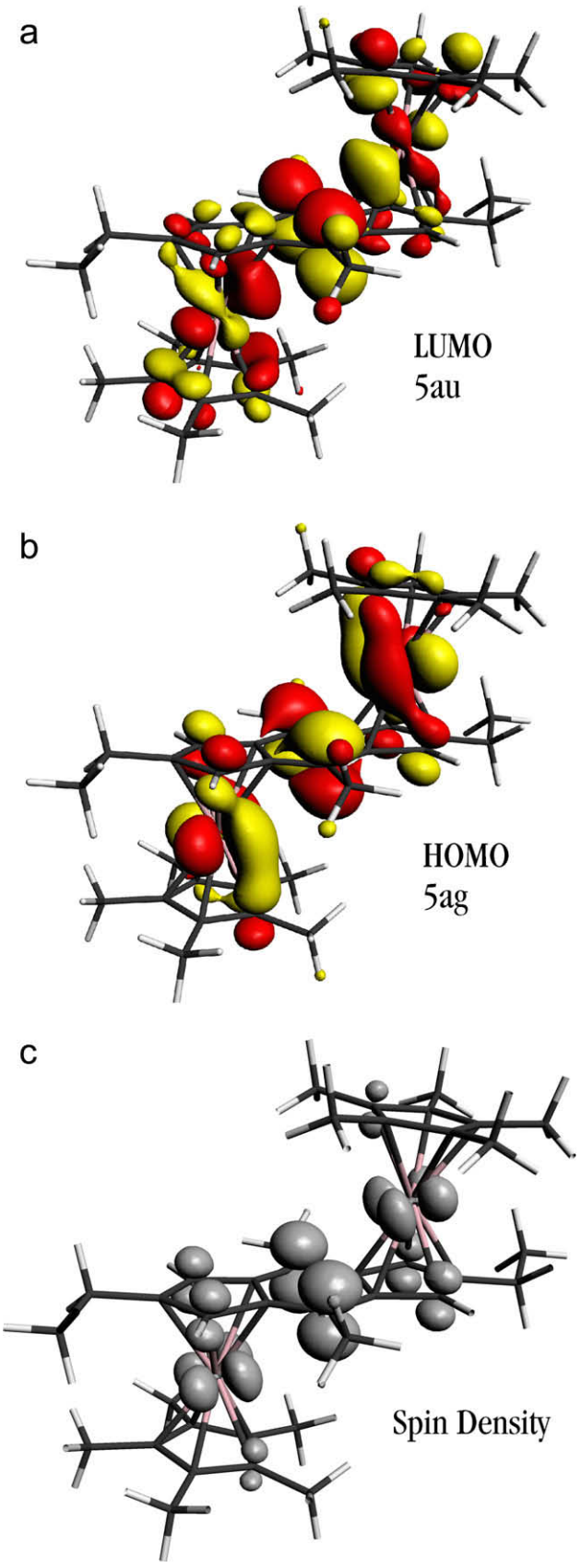

Fig. 6. (a) LUMO, (b) HOMO of **I** at 0.03 e/Å^3 and (c) spin density of $\mathbf{I}^+$ at 0.004 e/Å^3.

($\Delta g = 0.35$) [3], which denotes a higher degree of delocalization for $\mathbf{1}^+$.

Table 2
Calculated excitation energies (eV) and oscillator strength for **I** and $\mathbf{I}^+$ complexes.

	Wavelength (nm)		Energy (eV)	Oscillator strength ($\times 10^3$)	Symmetry	Composition (%)	Nature of the electronic transitions
	Exp.	Calc.					
I	626[a], 627[b]	694	1.79	13.31	^1A_u	96.9	5ag → 5au
	435[a], 436[b]	429	2.89	16.69	^1A_u	50.0	1ag → 5au
						48.3	5ag → 6au
	333[a], 329[b]	382	3.25	635.96	^1A_u	41.9	5ag → 6au
						41.9	1ag → 5au
$\mathbf{I}^+$	898[a], 901[b]	903	1.37	20.07	^1A_u	54.7	β 2au → β 5ag
						40.3	β 4ag → β 5ag
		899	1.38	26.57	^1A_u	51.0	β 4ag → β 5ag
						43.0	β 2au → β 5ag
		821	1.51	6.11	^1A_u	94.9	α 5ag → α 5au
	483[a], 486[b]	472	2.63	32.13	^1A_u	59.6	β 3au → β 5au
						21.0	β 4au → β 5au

[a] From a THF solution.
[b] From a DCM solution.

5. Density functional calculations

5.1. Molecular structure

As it can be seen in Table 1, the calculated geometrical parameters of **I** are in agreement with those obtained by X-ray diffraction for **1**. The most striking information is obtained in the analysis of the Ru–Cp* and Ru–Ic′ calculated distances, comparing both the neutral (**I**) and oxidized ($\mathbf{I}^+$) calculated species, in which the oxidation causes that ruthenium atoms come closer to the Ic′ ligand, thus increasing the interaction between them.

5.2. Molecular orbital analyses

A simplified molecular orbital (MO) diagram of the parent molecule [{CpRu}$_2$(Ic)] of C_{2h} symmetry is depicted in Fig. 5. This MO diagram exhibit the main features as that of its isoelectronic [{CpFe}$_2$(Ic)] [10] relative. The HOMO ($2b_g$) is essentially related to the non-bonding π_4 HOMO of Ic^{2-} with some CpRu admixture. This HOMO is well separated from the six "t_{2g}" metallic orbitals spanning as $2 \times a_g + b_g + a_u + 2 \times b_u$. The LUMO ($3b_u$) is a combination of a CpRu acceptor orbital with the Ic^{2-} LUMO. It is also energetically isolated. The significant computed HOMO–LUMO gap (1.46 eV) is consistent with the closed-shell configuration observed experimentally here for system **1**.

In the calculated neutral full molecule, [{Cp*Ru}$_2$(Ic′)] (**I**), the main features of the previous analysis are retained. The plot of the HOMO and LUMO isosurfaces of **I** and the Spin Density of the mixed-valent system, [{Cp*Ru}$_2$(Ic′)]$^+$[BF$_4$]$^-$ ($\mathbf{I}^+$), are presented in Fig. 6. The orbital composition analysis for **I** and $\mathbf{I}^+$ is presented in a Table as in a graphical form at the Supplementary data.

As can be seen from Fig. 6b, HOMO of **I** is composed by the Ic′ (32%) and Ru–Cp* (34% each) fragments in an equitative way. It must be noted the high participation of the Ic′ ligand into the LUMO, Fig. 6a, suggesting that an hypothetical radical anion, which will be isoelectronic with the *syn*-[{Fe(CO)$_3$}$_2$(Ic″)]$^+$[BF$_4$]$^{-(4,5)}$ can be obtained, and the presence of large hyperfine coupling constants shall indicate that the electron resides in an orbital with a large ligand character as the observed by O'Hare, in which the DFT calculations suggest a spin density of 32% over the Ic″ ligand. Broken Symmetry calculations have been carried out in order to ensure that we are in presence of a completely delocalized system. Starting from a strongly asymmetric molecule we force the system to be localized, however, always converge to a delocalized system.

Orbital composition analysis (see Tables in Supplementary data) shows that there exist several significant changes when the oxidation is carried out, which must be taken into account. Here we employ the unrestricted formalism for system $\mathbf{I}^+$. The SOMO (α ***5ag***) in which resides the unpaired electron presents an elevated contribution from the Ic′ fragment compared with the HOMO in the neutral molecule. Its unoccupied counterparts (β ***5ag***) also present an elevated contribution from the Ic′ fragment. The HOMO-1 (α and β of ***4au***) presents a slightly increasing of the contribution from the Ic′ fragment, the same is observed for HOMO-4 (α ***3ag***). These facts suggest that when the oxidation is carried out, an increasing of the interaction between the ruthenium and the Ic′ ligand is observed, also Ic′ acts as a bridging electronic ligand, allowing the exchange of the remanent electron between the two metallic centers, and for that reason the electronic density over the Ic′ ligand increases, and with it, the probability of finding the electron over it, as can be observed at the spin density of the oxidized system, Fig. 6c, with values of 25% for each Cp*Ru fragment and 50% for Ic′ fragment.

5.3. Time dependent density functional calculations

The calculated spectra of neutral complex shows several transitions, as is presented in Table 2. The calculated excitation at 382 nm presents the highest oscillator strength, which was assigned to a transition in which there exist a slight charge transfer from the Ic to both Cp*Ru fragments. The transition calculated at 694 nm, was assigned to a MLCT.

The calculated spectra for the oxidized complex ($\mathbf{I}^+$) shows the presence of several transitions. Those in the range from 821 to 903 nm contributes to the intervalence band (experimentally appears as a broad band between 680 and 1150 nm). Those calculated at 899 and 903 nm transitions occur between orbitals which present a large metallic character to an orbital which is delocalized over the entire molecule, these can be seen as a MLCT transition. In the case of the third calculated transition at 821 nm, this transition occurs between orbitals which have an extensive mixing of the Ic′ bridge and the metal centers, as it should be for an intervalence band according to the description given by Launay [32]. It must be noted that an intervalence band was not found in the neutral complex (**I**).

6. Conclusions

This work describes the synthesis and full characterization including X-ray structural analysis of a homobimetallic organome-

tallic system entitled as [{Cp*Ru}$_2$Ic′] (**1**) and the further oxidation affording a stable mixed-valent cation [{Cp*Ru}$_2$Ic′]$^+$[BF$_4$]$^-$ (**1**$^+$) which presents a strong electronic communication between metal sites as suggested by cyclic voltammetry, spectroscopic and DFT studies. This coupling results in a large electrochemical potential separation between successive one-electron redox events. The DFT calculations indicate that the oxidation of the neutral molecule occurs in an orbital that comprises the entire molecule, and the remanent electron is shared and delocalized between the two metallic moieties and the Ic′ bridging ligand. The mixed-valent system exhibit an intervalence charge transfer absorption band which was assigned by means of TD-DFT calculations.

Both experimental and theoretical facts demonstrate that the mixed valence system, is a delocalized one, and it can be classified as a Class III system according to Robin & Day classification.

Acknowledgements

The authors thank the financial support of: FONDECYT Grants 1060589, 1060588 and 1070345, Apoyo de tesis Doctoral CONICYT Grants N° 23070215 and 24080034, UNAB Grants UNAB-DI-02-09/R and UNAB-DI-09-09/I, PROJECT MILLENNIUM Grant No. P07-006–F. Also we thank the following Fellowships: Beca Doctoral CONICYT; Beca Doctoral UNAB.

Appendix A. Supplementary data

CCDC 736938 contains the supplementary crystallographic data for this paper. These data can be obtained free of charge via http://www.ccdc.cam.ac.uk/conts/retrieving.html, or from the Cambridge Crystallographic Data Centre, 12 Union Road, Cambridge CB2 1EZ, UK; fax: (+44) 1223-336-033; or e-mail: deposit@ccdc.cam.ac.uk. Supplementary data associated with this article can be found, in the online version, at doi:10.1016/j.poly.2009.12.002. Supplementary data associated with this article can be found, in the online version, at doi:10.1016/j.poly.2009.12.002.

References

[1] S. Barlow, D. O'Hare, Chem. Rev. 97 (1997) 637.
[2] A. Ceccon, S. Santi, L. Orian, A. Bisello, Coord. Chem. Rev. 248 (2004) 683.
[3] J.M. Manríquez, M.D. Ward, W.M. Reiff, J.C. Calabrese, N.L. Jones, P.J. Carroll, E.E. Bunel, J.S. Miller, J. Am. Chem. Soc. 117 (1995) 6182.
[4] D.R. Cary, C.G. Webster, M.J. Drewitt, S. Barlow, J.C. Green, D. O'Hare, Chem. Commun. (1997) 953.
[5] P. Roussel, D.R. Cary, S. Barlow, J.C. Green, F. Varret, D. O'Hare, Organometallics 19 (2000) 1071.
[6] E. Esponda, C. Adams, F. Burgos, I. Chavez, J.M. Manríquez, F. Delpech, A. Castel, H. Gornitzka, M. Rivière-Baudet, P. Rivière, J. Organomet. Chem. 691 (2006) 3011.
[7] Ch. Bonifaci, A. Ceccon, A. Gambaro, F. Manoli, L. Mantovani, P. Ganis, S. Santi, A. Venzo, J. Organomet. Chem. 577 (1998) 97, and references therein.
[8] W.L. Bell, C.J. Curtis, Ch.W. Eigenbrot Jr., C.G. Pierpont, J.L. Robbins, J.C. Smart, Organometallics 6 (1987) 266.
[9] C. Adams, C. Morales-Verdejo, V. Morales, D. Mac-Leod Carey, J.M. Manríquez, I. Chávez, A. Muñoz-Castro, F. Delpech, A. Castel, H. Gornitzka, M. Rivière-Baudet, P. Rivière, E. Molins, Eur. J. Inorg. Chem. (2009) 784.
[10] M.T. Garland, J.Y. Saillard, I. Chávez, B. Oëlckers, J.M. Manríquez, J. Mol. Struct. (THEOCHEM) 390 (1997) 199.
[11] W. Armarego, C. Chiai, Purification of Laboratory Chemicals, fifth ed., Elsevier, Butterworth, Heinemann, 2003.
[12] M.R. Dahrouch, P. Jara, L. Mendez, Y. Portilla, D. Abril, G. Alfonso, I. Chávez, J.M. Manríquez, M. Rivière-Baudet, P. Riviére, A. Castel, J. Rouzaud, H. Gornitzka, Organometallics 20 (2001) 5591.
[13] P.J. Fagan, W.S. Mahoney, J.C. Calabrese, I.D. Williams, Organometallics 9 (1990) 1843.
[14] G.M. Sheldrick, Shelxs 86, Program for the solution of Structure Resolution, University of Gottingen, Gottingen, Germany, 1986.
[15] G.M. Sheldrick, Shelxl 97, Program for the solution of Structure Refinement, University of Gottingen, Gottingen, Germany, 1997.
[16] ADF2008.01, Vrije Universiteit, Amsterdam, The Netherlands, SCM. <http://www.scm.com>.
[17] S.H. Vosko, L. Wilk, M. Nusair, Can. J. Phys. 58 (1980) 1200.
[18] J.P. Perdew, J.A. Chevary, S.H. Vosko, K.A. Jackson, M.R. Pederson, D.J. Singh, C. Fiolhais, Phys. Rev. B 46 (1992) 6671.
[19] E. van Lenthe, E.J. Baerends, J.G. Snijders, J. Chem. Phys. 101 (1994) 9783.
[20] G. Te Velde, F.M. Bickelhaupt, S.J.A. Van Gisberger, C. Fonseca Guerra, E.J. Baerends, J.G. Snijders, T.J. Ziegler, Comput. Chem. 22 (2001) 931.
[21] E. van Lenthe, E.J. Baerends, J. Comp. Chem. 24 (2003) 1142.
[22] A. Berces, R.M. Dickson, L. Fan, H. Jacobsen, D. Swerhone, T. Ziegler, Comput. Phys. Commun. 100 (1997) 247.
[23] H. Jacobsen, A. Berces, D. Swerhone, T. Ziegler, Comput. Phys. Commun. 100 (1997) 263.
[24] S.J.A. van Gisbergen, J.G. Snijders, E.J. Baerends, Comput. Phys. Commun. 118 (1999) 119.
[25] O.V. Gritsenko, P.R.T. Schipper, E.J. Baerends, Chem. Phys. Lett 302 (1999) 199.
[26] P.R.T. Schipper, O.V. Gritsenko, S.J.A. Van Gisbergen, E.J. Baerends, J. Chem. Phys. 112 (2000) 1344.
[27] F. Burgos, I. Chávez, J.M. Manríquez, M. Valderrama, E. Lago, E. Molins, F. Delpech, A. Castel, P. Rivière, Organometallics 20 (2001) 1287.
[28] M.D. Ward, in: A.J. Bard (Ed.), Electroanalytical Chemistry, Marcel Dekker, New York, 1989, p. 181.
[29] D. Osella, L. Milone, C. Nervi, M. Ravera, J. Organomet. Chem. 488 (1995) 1.
[30] G. Alfonso, I. Chávez, V. Arancibia, J.M. Manríquez, M.T. Garland, A. Roig, E. Molins, R.F. Baggio, J. Organomet. Chem. 620 (2001) 32.
[31] Y. Portilla, I. Chávez, V. Arancibia, B. Loeb, J.M. Manríquez, A. Roig, E. Molins, Inorg. Chem. 41 (2002) 1831.
[32] J.P. Launay, Chem. Soc. Rev. 30 (2001) 386, and references therein.